JOURNAL OF MATERIALS SCIENCE **39** (2004) 3375– 3381

Development and characterisation of SiAlON composites with TiB_2, TiN, TiC and TiCN

J. VLEUGELS, D. T. JIANG, O. VAN DER BIEST
Department of Metallurgy and Materials Engineering (MTM), Katholieke Universiteit Leuven, Kasteelpark Arenberg 44, B-3001 Leuven, Belgium
E-mail: jozef.vleugels@mtm.kuleuven.ac.be

30 vol% of TiB_2, TiCN, TiN or TiC was added to a sialon matrix with an X-phase sialon ($Si_{12}Al_{18}O_{39}N_8$) and an Al_2O_3-Si_3N_4 (77/23 wt%) starting powder composition and hot pressed at 1650°C in vacuum. The microstructures of the obtained composites were characterised by means of X-ray diffraction and electron microscopy, and the mechanical properties; E-modulus, hardness, bending strength and fracture toughness were measured and evaluated.

Fully dense composites with an X-phase sialon or a polyphase Al_2O_3–β-sialon–X-sialon matrix with 30 vol% of TiB_2, TiN and TiCN were obtained. TiC, added as a dispersed phase, however reacts with the nitrogen from the Si_3N_4 during liquid phase sintering, with the formation of $TiC_{1-x}N_x$, SiC and a changed sialon matrix composition. In the case of the X-phase sialon starting composition, a mullite matrix is obtained after sintering. The microstructural observations with respect to the sialon-TiC composites are found to be in agreement with the thermodynamic calculations.

1. Introduction

During the last 25 years, Si_3N_4-based ceramics have attracted much attention as structural ceramics because of their excellent thermal and mechanical properties. In the late 1970's, Si_3N_4-based ceramics entered the field of cutting tools. Their applicability nowadays is situated in turning nickel-based alloys and cast iron at high speeds [1, 2]. Even for drilling and reaming operations on grey cast iron, Si_3N_4-based tools are available these days [3]. For the machining of steels however, chemical dissolution-diffusion wear is limiting tool life [4].

At the high cutting speeds used with ceramics and the concomitant high temperatures at the cutting edge and the rake face of the tool, chemical interaction becomes the predominant wear mechanism. Recent investigation has shown that X-phase sialon and sialon ceramics with a high alumina content are less prone to chemical wear in turning steel than the commonly used commercial YSiAlON and SiAlON ceramics [5]. Although the above mentioned X-phase and high alumina content sialon ceramics are more chemically stable in contact with iron-based alloys, they have a lower abrasion wear resistance because of their modest fracture toughness and hardness [5, 6].

During the last five years, much attention was given towards the densification, microstructures and properties of Si_3N_4-TiN [7–16], Si_3N_4-TiC [7, 17–19], Si_3N_4-TiCN [7, 20, 21] and Si_3N_4-TiB_2 [22–26] composites. A review on particle silicon nitride-based composites is given by Gogotsi [27]. Despite the intensive research in this field, the Si_3N_4 materials of industrial interest have been mainly limited to YSiAlON ceramics with up to 5 wt% Y_2O_3 and/or 5 wt% Al_2O_3 as sinter additives.

Similarly to the developments in the field of the Al_2O_3-based cutting tools and the YSiAlON materials, this work is concerned with the toughening and hardening of X-phase sialon and sialon ceramics with a high Al_2O_3 content, by means of incorporating a secondary hard phase such as TiB_2, TiN, TiCN and TiC.

2. Experimental procedure

Commercial powders of Si_3N_4 (H. C. Starck grade LC 12-SX, particle size <0.5 μm), Al_2O_3 (Baikowski grade SM8, 100% <1 μm), SiO_2 (Sigma fumed silica), TiB_2 (H. C. Starck grade E, 1.5–2.0 μm), TiN (Ceramyg, 0.6–1.0 μm), TiCN (H. C. Starck grade C, 1.0–1.3 μm, C/N = 50/50) and TiC (Ceramyg, 0.2–0.5 μm) were used to prepare the starting powder mixtures of the ceramic composites.

Two types of sialon matrix were investigated. One having the X-phase sialon composition, $Si_{12}Al_{18}O_{39}N_8$ and further referred to as sialon X, was obtained by mixing Si_3N_4, Al_2O_3 and SiO_2 powder. The other matrix having a starting powder composition on the line between Si_3N_4 and Al_2O_3 in the Si_3N_4-AlN-Al_2O_3-SiO_2 phase diagram, as marked by (O) in Fig. 1. The latter ceramic is further referred to as sialon A. The starting powder compositions of the sialon materials are given in Table I.

To obtain homogeneous powder mixtures, 50–100 g powder was mixed on a multidirectional mixer (type turbula) for 72 h in 1 litre of n-propanol in a

TABLE I Starting powder composition of the sialon materials

	wt% Si_3N_4	wt% Al_2O_3	wt% SiO_2
Sialon A	22.73	77.27	0.00
Sialon X	18.72	58.88	22.40

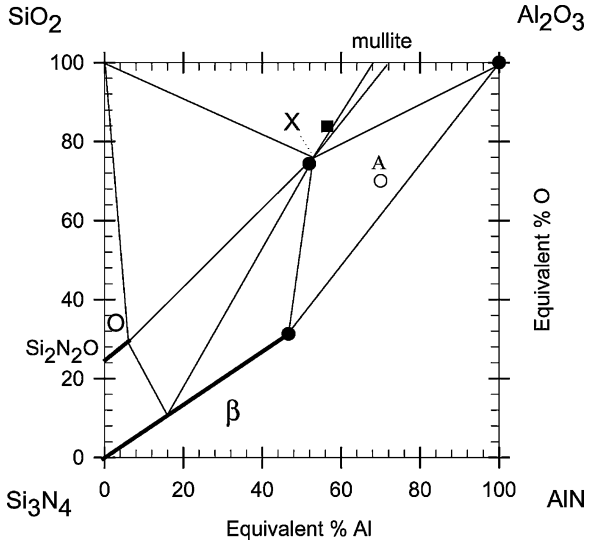

Figure 1 Chemical composition of the different sialon matrix phases (A and X), plotted in the Si_3N_4-AlN-Al_2O_3-SiO_2 phase diagram [30]. (○), the starting powder composition of sialon A (on the line between Si_3N_4 and Al_2O_3), (●), the chemical composition of the three different phases in the sintered sialon A. (X), the starting powder composition of sialon X and (■), the final composition of the X-phase in sialon X.

polyethylene bottle. The TiB_2, TiN, TiCN or TiC powders were added during the last 4 h of the mixing process. For some composites, addition of the secondary phases during the last 24 h of the mixing process was necessary to obtain a homogeneous microstructure. To break the agglomerates in the starting powders, 200 g alumina milling balls were added to the container. After mixing, the propanol was removed by means of a rotating evaporator.

The dry powder mixture was inserted into a graphite container with a diameter of 30 mm, coated with boron nitride. After cold pre-compression at 30 MPa, the samples were hot pressed in a FCT hot press (W 100/150-2200-50 LAX, FCT, Germany) under vacuum (10^{-4}–10^{-5} atm), during 1 h under a pressure of 28 MPa. The samples were separated from the furnace atmosphere by the graphite hot press set-up, whereas the sliding contacts were sealed by boron nitride. The ceramic samples were hot pressed at 1650°C, with a heating rate of 50°C/min, a cooling rate of 5°C/min till 1600°C and a cooling rate of 10°C/min down to room temperature.

Microstructural investigation was performed by scanning electron microscopy (SEM, FEI, XL30-FEG) and electron probe microanalysis (EPMA, Jeol 733 Superprobe). X-ray diffraction (XRD, Philips diffractometer equipped with a Cu-K_α source) analysis was used for phase identification.

The Vickers hardness, H_{V5} and H_{V10}, was measured on a Zwick hardness tester with a load of respectively 5 and 10 kg.

The fracture toughness, K_{IC5} and K_{IC10}, was obtained by the Vickers indentation technique, based on crack length measurements of the radial crack pattern produced by Vickers H_{V5} and H_{V10} indentations. The K_{IC} values were calculated according to the formula of Anstis [28].

The elastic modulus, E, of the ceramic specimens was measured by the resonance frequency method [29]. The resonance frequency was measured on a Grindo-Sonic (J. W. Lemmens Elektronika N. V., Leuven, Belgium).

The density of the specimens was measured in ethanol, according to the Archimedes method.

The flexural strength at room temperature was measured in a 3-point bending test. The test specimens (25.0 × 5.4 × 2.1 mm) were machined out of a hot pressed disc. All surfaces were ground with a Diamond Board MD40 75 B55 grinding wheel. The span width was 20 mm with a crosshead displacement of 0.1 mm/min. The reported values are the mean of at least three bending experiments.

3. Results and discussion

3.1. Microstructure of the composites

The hot pressed sialon A-TiX (70/30) composites, with TiX = TiB_2, TiN and TiCN, all reached their theoretical density. The density values used for the calculation of the theoretical density are 4.52 g/cm^3 for TiB_2, 5.43 g/cm^3 for TiN and 5.18 g/cm^3 for TiCN. The density of fully densified Sialon A and X was measured to be 3.55 and 3.09 g/cm^3 respectively. The density of the sialon X-TiN and sialon X-TiCN composites are very close to the calculated theoretical density and are considered as fully dense since no residual porosity could be observed by means of optical microscopy on polished cross-sections. In the sialon X-TiB_2 material however, a remaining porosity of about 2% was measured. The TiC-containing composites were all cracked.

XRD analysis revealed that the sintered Si_3N_4-Al_2O_3 ceramic, sialon A, is a polyphase material consisting of β-sialon, X-sialon and Al_2O_3. The SEM micrograph, shown in Fig. 2, clearly shows the presence of Al_2O_3 grains. The X-sialon and β-sialon phases however can not be distinguished in backscattered electron micrographs, because the difference in mean atomic number is too low. Since no residual microporosity was observed during SEM investigation, the sialon A material can be considered as fully dense.

The overall composition of the β-sialon phase, as obtained by XRD analysis is $Si_{2.77}Al_{3.23}O_{3.23}N_{4.77}$. Although the exact composition of the X-sialon phase could not be measured accurately by means of EPMA, because of the difficulty in distinguishing the β-sialon and X-sialon phases on backscattered electron images and because of the small size of the X-sialon regions, it is believed to be close to the reported literature value, $Si_{12}Al_{18}O_{39}N_8$ [30]. The starting powder composition and the chemical composition of the different phases after sintering at 1650°C are plotted on the phase diagram in Fig. 1.

Homogeneous sialon A-TiB_2, TiN and TiCN (70/30 vol% ratio) composites were obtained from powder mixtures that were mixed for 72 h. The secondary phase

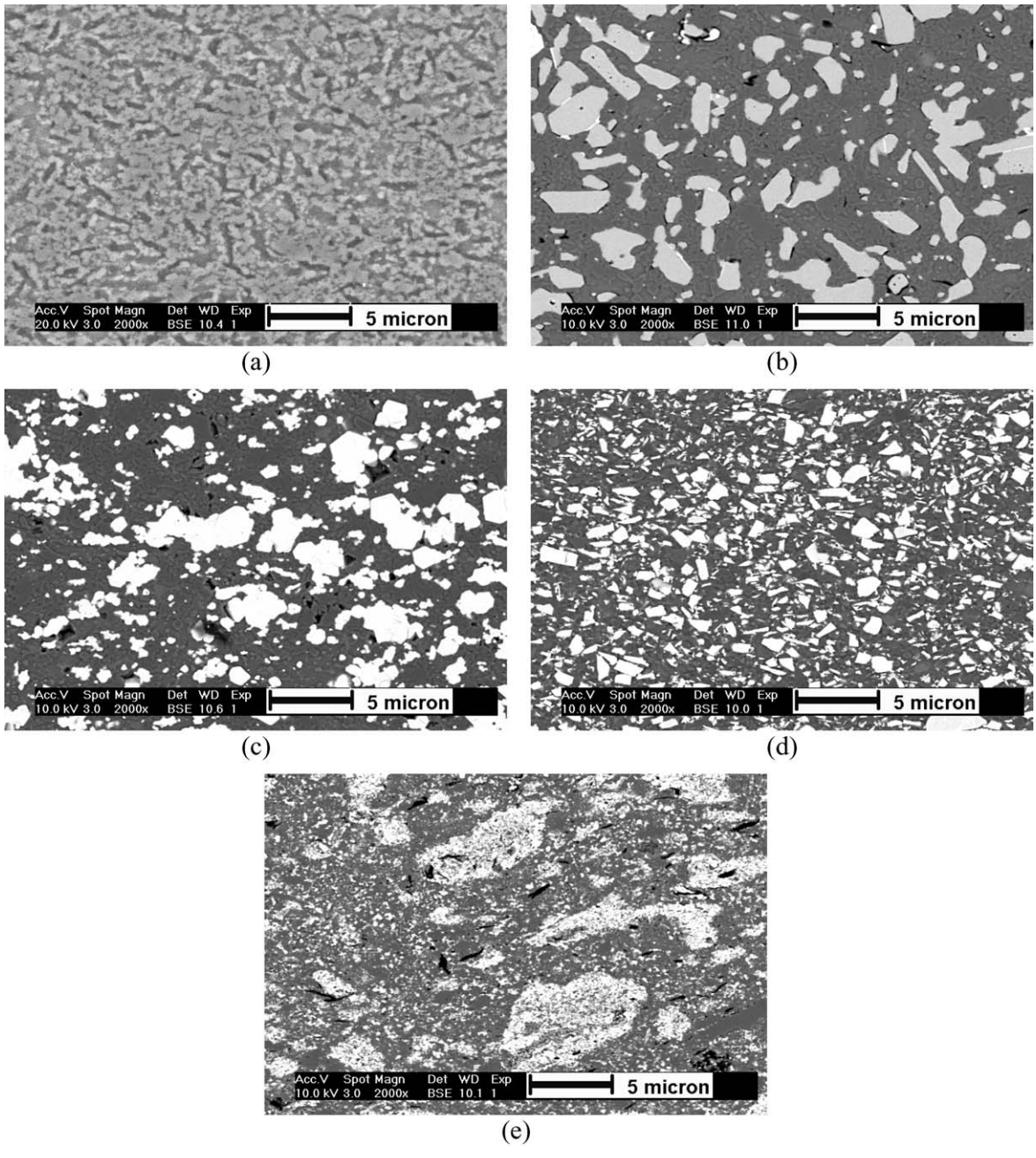

Figure 2 Microstructures of the sialon A-TiX (70/30) composites: (a) Sialon A, (b) A-TiB_2, (c) A-TiN, (d) A-TiCN and (e) A-TiC. The bright phase in Fig. a is α-Al_2O_3, whereas the dark phase represents β-sialon and X-phase sialon. The bright phase on the backscattered electron micrographs of the composites is the TiX phase.

was added during the last 4 h of the mixing procedure. The obtained sialon A-TiC composites on the contrary were not homogeneous and contained a substantial amount of large cracks. The microstructures of the sialon A-TiX (70/30) composites are shown in Fig. 2.

The X-ray diffraction patterns of sialon A and sialon A-TiX (70/30) composites are given in Fig. 3. A more detailed investigation, shown in Fig. 4, of the secondary phase in the composite with the sialon A-TiC starting powder composition shows that the secondary phase in the sintered composite is $TiC_{1-x}N_x$ instead of the expected TiC. No remaining TiC was detected. This indicates that TiC reacted with nitrogen from the Si_3N_4 powder during liquid phase sintering. From Figs 3 and 4, it is clear that the sintered sialon A-TiC specimen mainly contains Al_2O_3 as a matrix phase with $TiC_{1-x}N_x$ and SiC reaction products. Since the unit cell parameter of $TiC_{1-x}N_x$ solid solutions is a linear function of x [31], the composition of the reaction product in the sintered ceramic can be estimated from Fig. 5. The lattice parameters of TiN, TiC and the $TiC_{1-x}N_x$ product were obtained from the 2θ values of the (111) and (200) diffraction lines. The estimated composition of the $TiC_{1-x}N_x$ reaction product in the sialon A-TiC composite is $TiC_{0.3}N_{0.7}$.

The hot pressed sialon X ceramic consists mainly of X-phase sialon with a minor amount of Si_3N_4, as shown in Fig. 6. The chemical composition of the X-phase was determined by EPMA, using a pure SiO_2 and Al_2O_3 standard. Samples and standards were coated simultaneously with a very thin gold layer, to ensure a homogeneous coating thickness. Quantitative analysis was performed for Si, Al and O, N was calculated by difference.

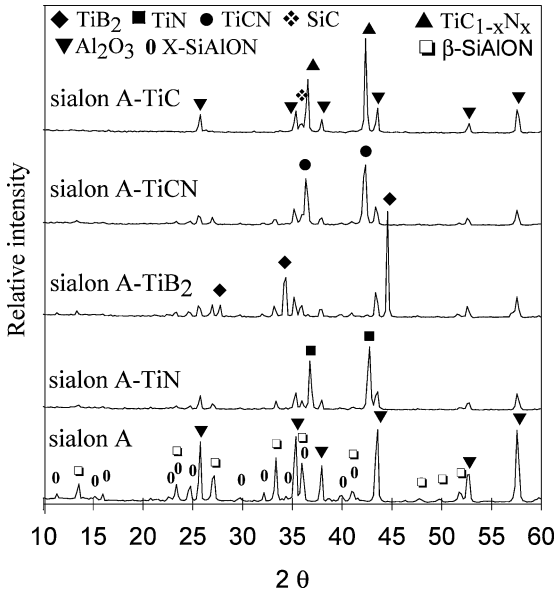

Figure 3 X-ray diffraction patterns of sialon A and the different sialon A-TiX (70/30) composites.

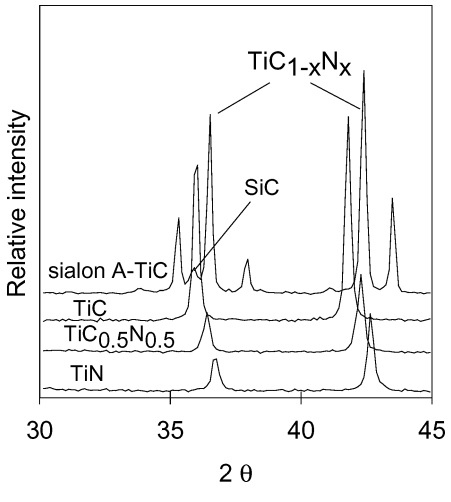

Figure 4 XRD-pattern of the sintered ceramic with sialon A-TiC (70/30) starting powder composition, together with the diffraction patterns of the TiC, $TiC_{0.5}N_{0.5}$ and TiN powders.

Its composition was found to be $Si_{14.1}Al_{24.5}O_{54.4}N_{7.0}$, which is more towards the mullite side in the phase diagram (see Fig. 1) [32]. The Si_3N_4 crystals were identified as α-Si_3N_4 by means of transmission electron microscopy, and are tought to be nucleation sites for X-phase sialon during liquid phase sintering [32]. No porosity was observed during SEM investigation.

Homogeneous sialon X-TiB_2 and sialon X-TiN composites were obtained after 72 h of mixing, the secondary phase was added during the last 24 h. Homogeneous sialon X-TiCN composites were already obtained with addition of the TiCN during the last 4 h of the mixing procedure. The sialon X-TiC composites were not homogeneous and contained cracks. The microstructures of the sialon X-TiX (70/30) composites are shown in Fig. 6. The grain size of the TiB_2 phase is much larger than that of TiN and TiCN.

The X-ray diffraction patterns of sialon X and sialon X-TiX (70/30) composites are given in Fig. 7. The diffraction pattern of the sialon X-TiC composite

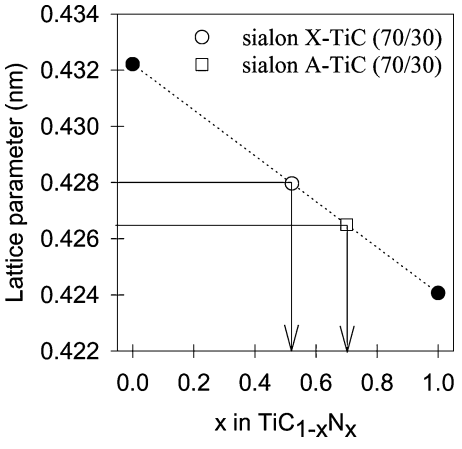

Figure 5 Lattice parameter of $TiC_{1-x}N_x$ as a function of x.

clearly shows that the obtained matrix composition is mullite instead of the expected X-phase sialon, with a $TiC_{1-x}N_x$ secondary phase and a minor amount of SiC. From this, it is clear that the TiC powder reacted with the nitrogen of the Si_3N_4 to form $TiC_{1-x}N_x$ during liquid phase sintering, thereby shifting the composition of the matrix phase towards mullite. The estimated composition of the $TiC_{1-x}N_x$ reaction product is $TiC_{0.5}N_{0.5}$, as shown in Fig. 5.

3.2. *In-situ* reactions in TiC-containing composites

With respect to the formation of $TiC_{1-x}N_x$ in the sialon A-TiC and sialon X-TiC composites, this reaction may be explained via the thermodynamic stability of the phases of interest.

Based on the microstructural analysis of this work and the experimental evidence for the presence of SiC in Si_3N_4-TiC composites found elsewhere [17], the following reaction can be assumed:

$$3TiC + xSi_3N_4 \Leftrightarrow 3TiC_{1-x}N_x + 3xSiC + x/2N_2 \quad (1)$$

Although the X-sialon phase is formed *in-situ* during sintering of the sialon X-TiC composites, it is interesting to consider the following reaction as well

$$6TiC + xSi_{12}Al_{18}O_{39}N_8 \Leftrightarrow 6TiC_{1-x}N_x + 3x3Al_2O_3 \cdot 2SiO_2 + 6xSiC + xN_2 \quad (2)$$

The energy of formation of X-sialon, $Si_{12}Al_{18}O_{39}N_8$, was calculated according to the method of Hillert [33], the data for Si_3N_4, TiC and TiN were taken from Barin [34]. The thermodynamic data for mullite, $3Al_2O_3{\cdot}2SiO_2$, were taken from the JANAF tables [35]. Assuming that $TiC_{1-x}N_x$ solid solution can be considered as ideal solutions of TiN and TiC, the energy of formation can be calculated as:

$$\Delta G^{\circ}_{TiC_{1-x}N_x} = x\Delta G^{\circ}_{TiC} + (1-x)\Delta G^{\circ}_{TiN} + RT\{x\ln x + (1-x)\ln(1-x)\} \quad (3)$$

with

$$\Delta G^{\circ}_{TiC} = -44317 + 3.522\ T\ (\text{cal/mole})\ [24] \quad (4)$$

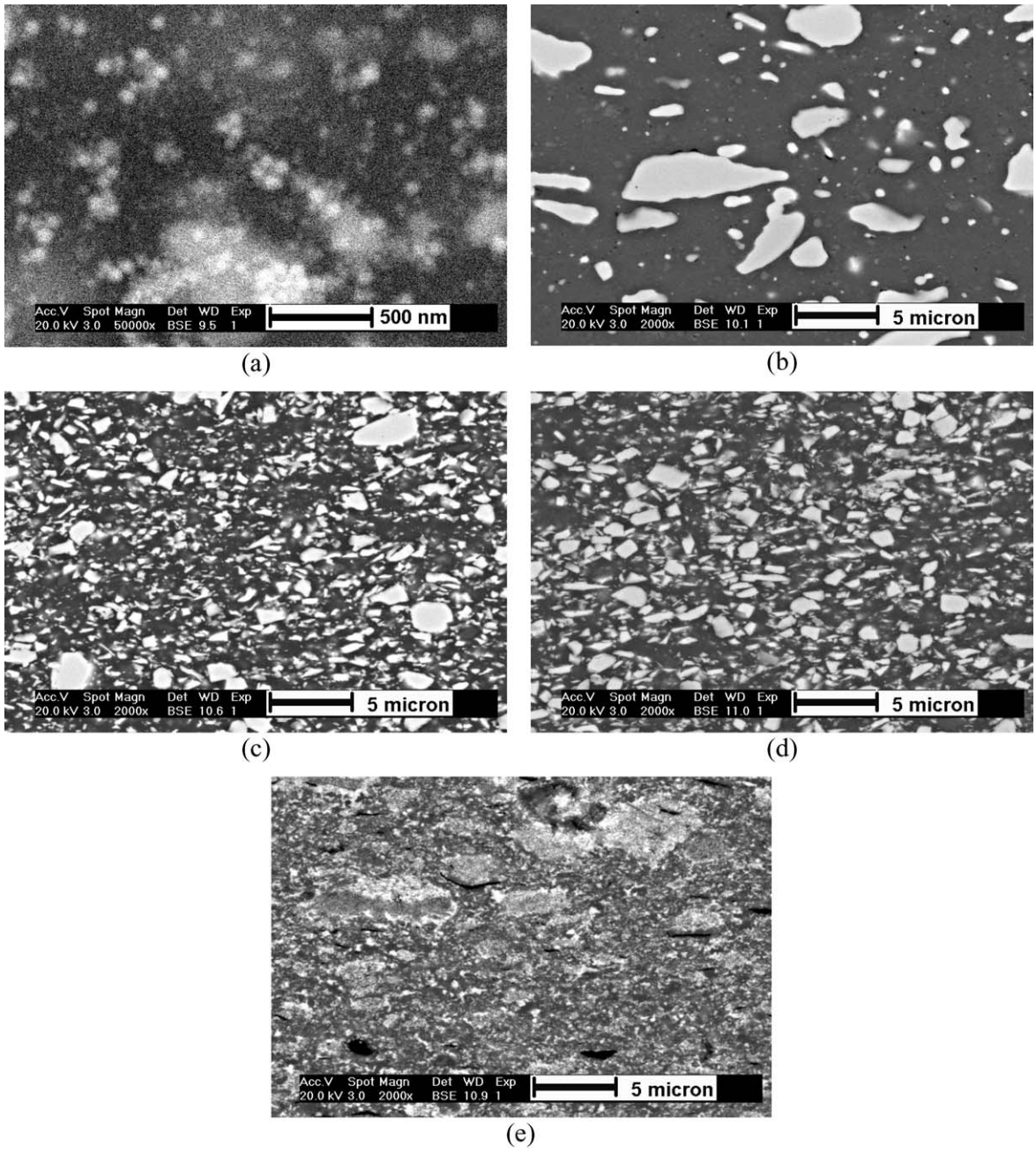

Figure 6 Microstructures of the sialon X-TiX (70/30) composites: (a) Sialon X, (b) X-TiB_2, (c) X-TiN, (d) X-TiCN and (e) X-TiC. The bright phase in Fig. a is residual Si_3N_4. The bright phase on the backscattered electron micrographs of the composites is the TiX phase.

and

$$\Delta G^{\circ}_{\mathrm{TiN}} = -80638 + 22.604\ \mathrm{T}\ (\mathrm{cal/mole})\ [24] \quad (5)$$

The calculated equilibrium nitrogen pressures for reaction (1) and (2) are plotted versus the $TiC_{1-x}N_x$ solid solution composition in Fig. 8. According to the data in Fig. 8, TiC will react with Si_3N_4 under the experimental conditions. The formation of $TiC_{1-x}N_x$ will proceed until all Si_3N_4 is consumed or until all TiC is converted into TiN. Fig. 8 also shows that X-phase sialon is not stable in contact with TiC under the experimental nitrogen pressures. A maximum calculated equilibrium substitution level, x, for the $TiC_{1-x}N_x$ phase is 0.43, which is in relatively good agreement with the composition of $TiC_{0.48}N_{0.52}$ that was measured by means of XRD.

The substitution level measured for the $TiC_{1-x}N_x$ phase in the sialon A-TiC material was higher than in the sialon X-TiC ceramic. Although it is not possible to predict a maximum equilibrium substitution level because of the uncertainty about the exact reaction products, it can be assumed that the log P_{N2} curve for the reaction of $Si_{2.77}Al_{3.23}O_{3.23}N_{4.77}$, the β-sialon phase of sialon A, with TiC will be between that of reaction (1) and (2), because of the intermediate energy of formation of the β-sialon phase. This would explain the higher x value of 0.70 for the $TiC_{1-x}N_x$ phase in the sialon A-TiC composite.

3.3. Mechanical properties

The mechanical properties of sialon A, sialon X and their composites are given in Table II. Sialon

TABLE II Mechanical properties of sialon X, sialon A and the sialon-TiX (70/30) composites

	H_{V5} (kg/mm^2)	H_{V10} (kg/mm^2)	E (GPa)	K_{IC} (5 kg) (MPa $\sqrt{m}$)	K_{IC}(10 kg) (MPa $\sqrt{m}$)	ρ (g/cm^3)	Relative ρ%	σ_B (MPa)
X	1252 ± 39	/	213	1.2	/	3.09	100.0	254 ± 20
X-TiN	1334 ± 26	1328 ± 27	284	2.9 ± 0.1	3.2 ± 0.3	3.77	99.5	381 ± 64
X-TiB_2	1301 ± 28	1247 ± 7	255	3.2 ± 0.6	4.1 ± 0.6	3.46	98.3	277 ± 10
X-TiCN	1399 ± 23	1360 ± 23	257	2.3 ± 0.1	2.5 ± 0.3	3.73	100.0	408 ± 24
X-TiC	inhomogeneous mullite-$TiC_{1-x}N_x$ composite with cracks							
A	1579 ± 36	1636 ± 41	277	2.1 ± 0.1	2.3 ± 0.1	3.55	100.0	373 ± 85
A-TiN	1526 ± 43	1529 ± 37	360	2.9 ± 0.2	3.4 ± 0.3	4.15	100.0	376 ± 88
A-TiB_2	1488 ± 72	1486 ± 42	296	3.6 ± 0.3	3.6 ± 0.2	3.80	99.0	378 ± 50
A-TiCN	1677 ± 27	1634 ± 29	334	2.5 ± 0.1	2.7 ± 0.2	4.03	100.0	314 ± 128
A-TiC	inhomogeneous sialon-$TiC_{1-x}N_x$ composite with cracks							

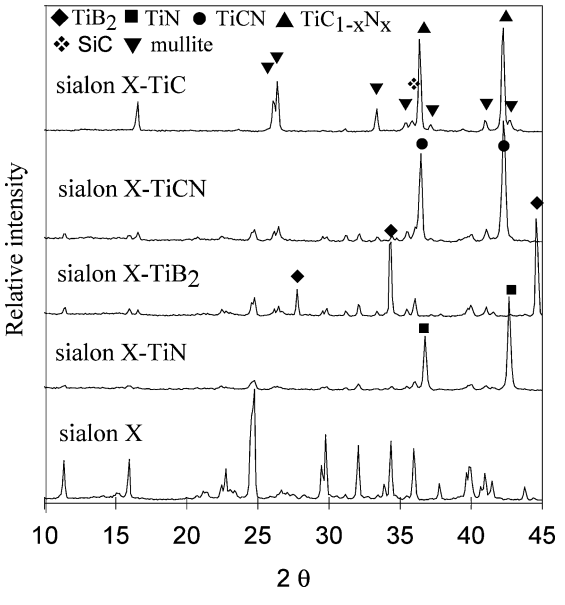

Figure 7 X-ray diffraction patterns of sialon X and the different sialon X-TiX (70/30) composites.

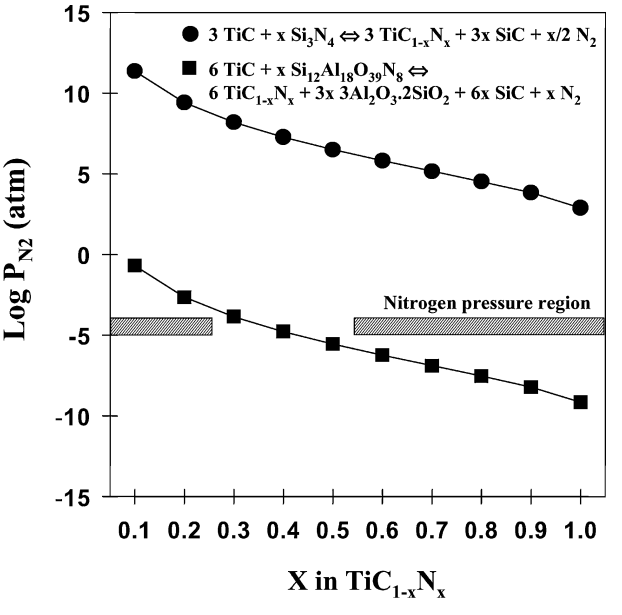

Figure 8 Calculated equilibrium nitrogen pressures at 1650°C for reaction 7 and 8.

A is a polyphase material with high hardness of 1636 kg/mm^2, a reasonable room temperature bending strength of 373 MPa and a modest fracture toughness of 2.3 MPa$\sqrt{m}$. Due to the high Al_2O_3 content, the hardness of Sialon A is higher than that of the constituent X-phase sialon and β-SiAlON ($Si_{2.77}Al_{3.23}O_{3.23}N_{4.77}$). The hardness is comparable to that of single-phase β-$Si_{6-z}Al_zO_zN_{8-z}$ with $z < 1.0$ but lower than that of α-SiAlON containing Y_2O_3 [36]. The high hardness of sialon A remains in the sialon A-TiCN composites, but is lower for the sialon A-TiB_2 and -TiN ceramics. The toughness of the sialon A-TiCN composite is comparable to that of sialon A, which is comparable to that of single phase β-$Si_{6-z}Al_zO_zN_{8-z}$ with $z < 2.0$ and the upper values for α-SiAlON with Y_2O_3 [36]. The toughness of the sialon A-TiB_2 and sialon A-TiN materials is higher. The addition of 30 vol% of TiB_2, TiCN or TiN has no influence on the bending strength of sialon A.

Pure X-phase sialon, sialon X, has a modest hardness of 1250 kg/mm^2, a fracture toughness of 1.2 MPa$\sqrt{m}$ and a bending strength of 250 MPa. These experimental data are comparable with the reported literature data on X-phase sialon [32, 37, 38].

Addition of TiN and TiCN slightly increases the hardness, whereas the addition of 30 vol% of TiB_2 has only a minor effect on the hardness, probably because of the extended grain growth of the TiB_2 phase. The bending strength of sialon X-TiB_2 is comparable with that of sialon X. The sialon X-TiN and sialon X-TiCN materials have a higher strength. The fracture toughness of sialon X is almost doubled by the addition of TiCN. An even higher toughness was obtained by the addition of TiN and the toughest composites were obtained with TiB_2. The predominant toughening mechanism in the sialon X-TiX (70/30) composites is crack deflection.

The hardness of the sialon A-TiN and -TiCN composites is higher than reported for Si_3N_4 composites with 30 vol% TiN [27], but the fracture toughness is significantly lower [11, 20, 27], due to the high hardness but modest toughness of the Sialon A matrix. The hardness of the sialon A-TiB_2 composite is comparable to that reported for a HIPed Si_3N_4-TiB_2 composite with 30 vol% TiB_2, but the fracture toughness is substantially lower [26]. The hardness and toughness of the sialon X based composites is inferior to that of the reported Si_3N_4-TiN [8, 20, 27] and -TiB_2 [26] composites.

4. Conclusions

Fully dense composites with an X-phase sialon or a polyphase Al_2O_3–β-sialon–X-sialon matrix with 30 vol% of TiB_2, TiN and TiCN dispersed phases can be obtained by conventional hot pressing in vacuum at 1650°C.

TiC, added as a dispersed phase, however reacts with the nitrogen from the Si_3N_4 during liquid phase sintering, with the formation of $TiC_{1-x}N_x$, SiC and a changed sialon matrix composition. In the case of the X-phase sialon starting composition, a mullite matrix is obtained after sintering. These microstructural observations are found to be in agreement with thermodynamic calculations.

The sialon A-TiX (70/30) composites have a high hardness (1500–1700 kg/mm^2) and a reasonable bending strength (370 MPa). The fracture toughness of the sialon A-TiN and TiB_2 materials is ± 3.5 MPa$\sqrt{\text{m}}$. The toughness of sialon A and the sialon A-TiCN composite is lower (2.5 MPa$\sqrt{\text{m}}$).

The hardness of the sialon X-TiX (70/30) composites (1300–1400 kg/mm^2) is significantly lower than that of the sialon A-TiX materials. The toughness and bending strength are functions of the type of secondary phase.

References

1. T. N. BLACKMAN, *Foundryman* **3** (1990) 17.
2. J. AUCOTE and S. R. FOSTER, *Mater. Sci. Tech.* **2** (1986) 700.
3. K. G. GÜHRING, "Product Catalogue" (Sigmaringen-Laiz, Germany).
4. S. T. BULJAN and F. WAYNE, *Wear* **133** (1989) 309.
5. J. VLEUGELS, P. JACOBS, J. P. KRUTH, P. VANHERCK, W. DU MONG and O. VAN DER BIEST, *ibid.* **189** (1995) 32.
6. J. VLEUGELS and O. VAN DER BIEST, *J. Eur. Ceram. Soc.* **13**(6) (1994) 529.
7. M. HERRMANN, C. SCHUBERT, W. HERMEL, E. MEIßNER and G. ZIEGLER, *CFI/Ber. DKG* **73**(7/8) (1996) 434.
8. T. EKSTRÖM, *J. Eur. Ceram. Soc.* **13** (1994) 551.
9. G. HILLINGER and V. HLAVACEK, *J. Amer. Ceram. Soc.* **78**(2) (1995) 495.
10. F. HONG, R. J. LUMBY and M. H. LEWIS, *J. Eur. Ceram. Soc.* **11** (1993) 237.
11. A. BELLOSI, S. GUICCIARDI and A. TAMPIERI, *ibid.* **9** (1992) 83.
12. F. DESCHAUX-BEAUME, T. CUTARD, N. FRETY and C. LEVAILLANT, *J. Amer. Ceram. Soc.* **85** (2002) 1860.
13. J. L. HUANG, F. C. CHOU and H. H. LU, *J. Mater. Res.* **12** (1997) 2357.
14. H. J. CHOI, K. S. CHO and J. G. LEE, *J. Amer. Ceram. Soc.* **80** (1994) 2681.
15. Y. G. GOGOTSI and G. GRATHWOHL, *J. Mater. Sci.* **28** (1993) 4279.
16. N. UCHIDA and M. KOIZUMI, *J. Amer. Ceram. Soc.* **68** (1985) C-38.
17. J. L. HUANG, H. L. CHIU and M. T. LEE, *ibid.* **77** (1994) 705.
18. Y. CHIH-HUNG and H. MIN-HSIUNG, *ibid.* **78** (1995) 2395.
19. S. T. BULJAN and S. F. WAYNE, *Adv. Ceram. Mater.* **2**(4) (1987) 813.
20. M. HERRMANN, B. BALZER, C. SCHUBERT and W. HERMEL, *J. Eur. Ceram. Soc.* **12** (1993) 287.
21. J. T. LI, W. S. LIU, Y. L. XIA and C. C. GE, *J. Mater. Res.* **11**(1996) 2968.
22. T. C. ARTHURS, H. MOSTAGHACI and J. G. MURPHY, *Ceram. Eng. Sci. Proc.* **11**(9/10) (1990) 1778.
23. F. HONG and M. H. LEWIS, *ibid.* **14**(9/10) (1993) 699.
24. B. Y. SHEW and J. L. HUANG, *Mater. Sci. Eng.* A **159** (1992) 127.
25. J. L. HUANG, F. J. KUO and S. Y. CHEN, *ibid.* A **174** (1994) 157.
26. A. H. JONES, R. S. DOBEDOE and M. H. LEWIS, *J. Eur. Ceram. Soc.* **21** (2001) 969.
27. Y. G. GOGOTSI, *J. Mater. Sci.* **29** (1994) 2541.
28. G. R. ANSTIS, P. CHANTIKUL, B. R. LAWN and D. B. MARSHALL, *J. Amer. Ceram. Soc.* **64** (1981) 533.
29. ASTM C 1259–94: Standard Test Method for Dynamic Young's Modulus, Shear Modulus, and Poisson's Ratio for Advanced Ceramics by Impulse Excitation of Vibration (ASTM, May 1994).
30. I. K. NAIK, L. J. GAUCKLER and T. Y. TIEN, *J. Amer. Ceram. Soc.* **61**(7/8) (1978) 332.
31. H. PASTOR, *Mater. Sci. Eng.* A **105/106** (1988) 401.
32. Y. ZHOU, J. VLEUGELS, T. LAOUI, P. RATCHEV and O. VAN DER BIEST, *J. Mater. Sci.* **30** (1995) 4584.
33. M. HILLERT and S. JONSSON, *Z. Metallkd.* **83** (1992) 720.
34. I. BARIN, "Thermochemical Data of Pure Substances" (VCH Verlagsgesellschaft GmbH, Weinheim, Germany, 1993).
35. D. R. STULL and H. PROPHET, "JANAF Thermochemical Table," 2nd ed. (Office of Standard Reference Data, National Bureau of Standards, Washington DC, 1971).
36. T. EKSTRÖM and M. NYGREN, *J. Amer. Ceram. Soc.* **75**(2) (1992) 259.
37. C. C. ANYA and A. HENDRY, *J. Mater. Sci.* **29** (1994) 527.
38. C. C. SHEPPARD, K. J. D. MACKENZIE and M. J. RYAN, *J. Eur. Ceram. Soc.* **18** (1998) 185.

Received 2 May 2003
and accepted 29 January 2004